Nature Environment and Pollution Technology
An International Quarterly Scientific Journal

p-ISSN: 0972-6268
(Print copies up to 2016)
e-ISSN: 2395-3454

Vol. 23 | No. 1 | pp. 321-330 | 2024

Original Research Paper

https://doi.org/10.46488/NEPT.2024.v23i01.027

Open Access Journal

A Facile Method for Synthesis of α-Fe_2O_3 Nanoparticles and Assessment of Their Characterization

Paramjeet Dhull*, Rajesh Kumar Lohchab*†, Mikhlesh Kumari*, Kulbir Singh, Anil Kumar Bhankhar*** and Shaloo******

*Department of Environmental Science and Engineering, Guru Jambheshwar University of Science and Technology, Hisar-125001, Haryana, India

**Department of Civil Engineering, MM Engineering College, Maharishi Markandeshwar (Deemed to be University), Mullana (Ambala), 133207, Haryana, India

***Department of Bio and Nanotechnology, Guru Jambheshwar University of Science & Technology, Hisar-125001, Haryana, India

****Water Technology Centre, ICAR-Indian Agricultural Research Institute, New Delhi-110012, India

†Corresponding Author: Rajesh Kumar Lohchab; rajeshlohchab@gmail.com

Nat. Env. & Poll. Tech.
Website: www.neptjournal.com

Received: 20-06-2023
Revised: 13-08-2023
Accepted: 19-08-2023

Key Words:
α-Fe_2O_3 nanoparticles,
Hematite
XRD
SEM-EDX
Raman spectroscopy
BET

ABSTRACT

Recently, magnetic nanomaterials have gained much attention from researchers because of their various unique physical and chemical properties and usage in a wide range of technological aspects. In this study, the synthesis of α-Fe_2O_3 nanoparticles was performed by a simple co-precipitation method. The synthesis of α-Fe_2O_3 nanoparticles was carried out by mixing ferric nitrate and oxalic acid in an aqueous solution followed by evaporation, resulting in the solution's dried form. The synthesized nanoparticles were analyzed by XRD, FTIR, Raman spectra, SEM-EDX, DSC, BET, and Zeta potential for detailed examination of the morphology, structure, and other physicochemical characteristics. The XRD results confirmed that the nanoparticles formed were Hematite (α-Fe_2O_3) after the evaluation of obtained spectra compared to the Joint Committee on Powder Diffraction Standards Database (JCPDS). The FTIR spectra showed various bonds among functional groups, O-H bending, Fe-O group, and within-vibration bonds. The phase study of the α-Fe_2O_3 nanoparticles was performed by using Raman spectroscopy. SEM depicted a sphere-like or rhombohedral (hexagonal) structure, and the EDX spectrum confirmed the peaks of iron and oxygen.

INTRODUCTION

Nanotechnology, engineering, and manufacturing art of working and functionating matter at the nanoscale (1–100 nm) has emerged as an attractive option in the field of engineering and environmental science. Nanotechnology has a great beneficial potential in a wide range of fields (Lo et al. 2012) like biomedicine (Ebrahiminezhad et al. 2016), biotechnology, enzyme and protein immobilization, biosensors (Morais et al. 2009), wastewater treatment, bioremediation of heavy metals (Xu et al. 2022), optics, ceramics, electronics (Rao et al. 2000) and environmental remediation (Villanueva et al. 2009). It has been considered that nanoparticles, mainly metal oxides, are working more effectively and efficiently as adsorbents for cleaning environmental pollution because of their smaller size, large surface area, and zero generation of secondary pollutants. They can penetrate deeper contamination zones where microparticles cannot (Gurlhosur & Sreekanth 2018). Nanotechnology has been touted as a modern technology that helps in outstripping various physical and chemical property barriers of different materials in nano-forms (Masoomi et al. 2010). The synthesis of nanomaterials can be attempted by different methods like photochemical reduction, chemical reduction, spray-pyrolysis, electrodeposition, hydrothermal, co-precipitation, sol-gel, and microemulsion (Bozkurt 2020).

In recent times, iron oxide nanoparticles have attracted great attention due to their excellent thermodynamic properties, strong environmental toxicity, resistance to biological toxicity and corrosion, high stability, strong redox potential, and absorption abilities (Liu et al. 2019). Due to their unique physical properties as compared to clump material, magnetic nanoparticles have gained significant interest. The properties of a nanomaterial are greatly influenced by surface morphology, phase, and microstructure as compared with those of clump materials. However, these parameters are dependent on the quality and purity of the

phase of the synthesized nanomaterial (Qureshi et al. 2022). As a result, the importance of single-phase material can not be emaciated as it is vital for the specific measurement of different physical properties (magnetic and electrical, etc.) (Terayama et al. 2018).

Iron oxide is a renowned conventional semiconductor with a negative temperature resistance coefficient (Terna et al. 2021). The quest to prepare a homogenous mixture of iron nanoparticles has led researchers to develop various practices for the manufacturing process of iron oxide nanoparticles, such as chemical precipitation, sol-gel process, pulsed layer ablation, electro-spinning and solvent precipitation, hydrothermal, combustion technique, etc. (Farahmandjou & Soflaee 2015, Ganguli & Tokeer 2007, Subaihi & Naglah 2022). The pathway used for the synthesis of nanomaterial greatly influences the standardized physicochemical characterization of magnetite nanoparticles by affecting the crystallinity, structure, and surface area (Chircov & Vasile 2022). However, there is still a major challenge in the development of a simple and more efficient method for the synthesis of pure and homogenous magnetite particles with high dispersion and narrow-size dispensation (Terayama et al. 2018). There are two familiar crystalline phases of iron oxide (Fe_2O_3), i.e., the γ-phase has a cubic structure, maghemite, and the α-phase has a rhombohedral structure, hematite (Wang et al. 2013). The process of calcination performs the conversion of γ-phase to α-phase when the temperature reaches 400°C, and this forms α-Fe_2O_3 nanoparticles with significant grain growth (Farahmandjou & Soflaee 2015). The α-phase is considered to be the most important polymorph existing as hematite with a rhombohedral-centered hexagonal structure and a close-packed oxygen lattice (Basavegowda et al. 2017). Hematite (α-Fe_2O_3), the most stable form of iron oxide, is one of the most environment-friendly semiconductors having a band gap energy of Eg = 2.1 eV (Cao et al. 2003). It is conventionally used for gas sensors, catalysts, fine ceramics, electrodes, magnetic materials, photocatalytic activity, red pigment, and anticorrosion protective paints (Farahmandjou & Soflaee 2015). While synthesizing iron nanoparticles, some important factors must be considered, such as the size and shape of nanoparticles, intrinsic properties, surface charge and surface coating, non-toxicity, and their stability in the aqueous environment (Chircov & Vasile 2022). Therefore, the choice of a suitable synthesis method offers the ability to control the shape, size, stability, and surface coating of the nanoparticles (Ansari et al. 2022). The salt (precursor) and reactants ratio used in the chemical

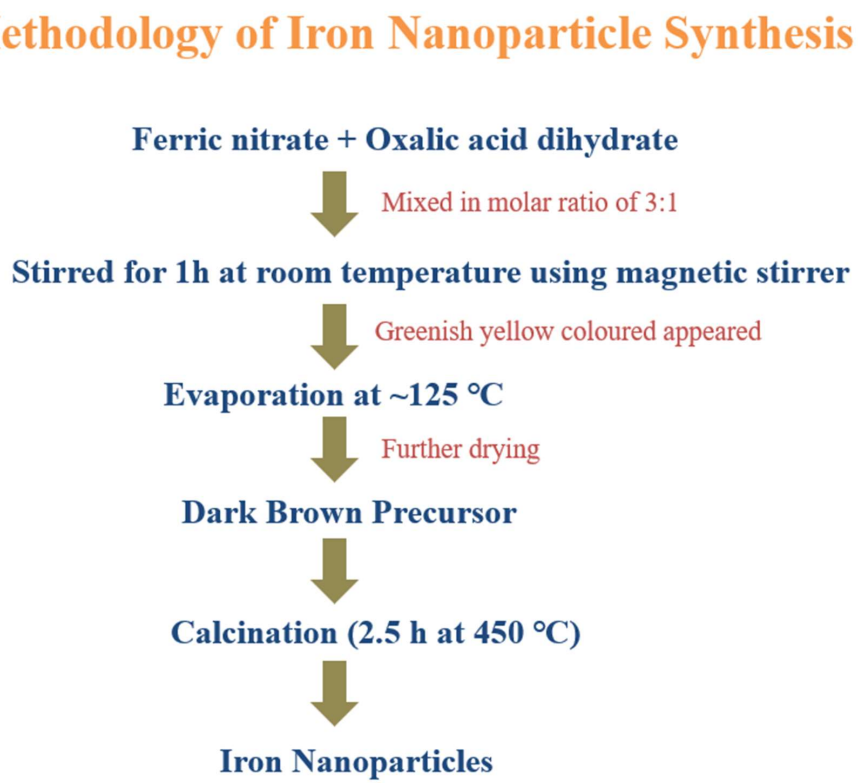

Fig. 1: Flow diagram of α-Fe_2O_3 nanoparticles synthesis.

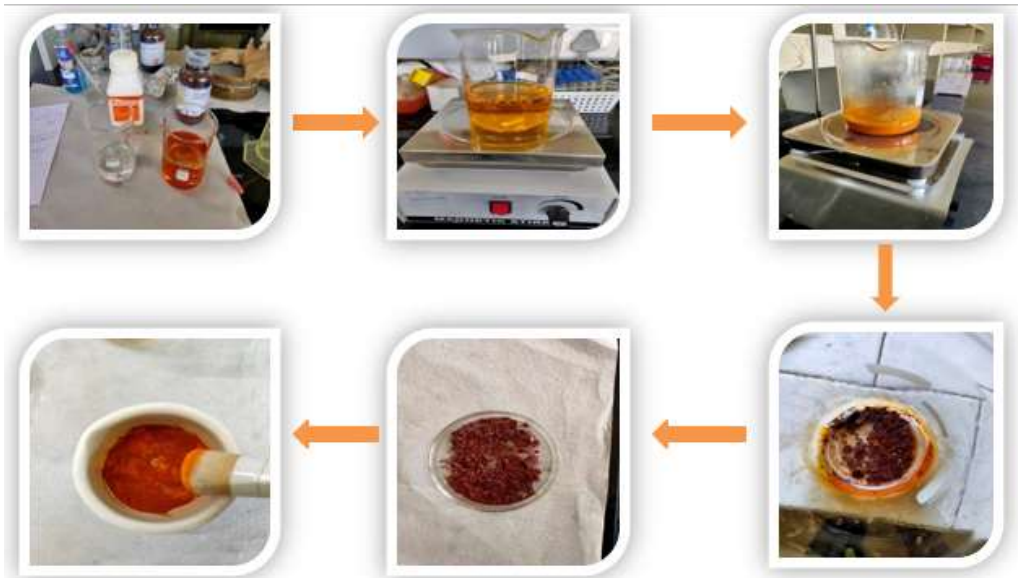

Fig. 2: Pictorial representation of methodology of α-Fe_2O_3 nanoparticles synthesis.

methods of iron nanoparticle synthesis greatly influences its composition, size, shape, and ionic strength. The mixing rate and the temperature provided during the process, along with the agitation provided, also influence the properties of the iron nanoparticles formed (Aragaw et al. 2021).

In the present study, iron oxide nanoparticles were synthesized by a simple chemical method. Analytical grade chemicals (Ferric nitrate and Oxalic acid) were used as the initial compounds, along with water as a solvent for the synthesis of nano-sized, single-phase hematite (α-Fe_2O_3). The morphological and structural characterization was performed by SEM-EDX, FTIR, XRD and Raman spectroscopy, DSC, BET, and Zeta potential.

MATERIALS AND METHODS

Synthesis Procedure of α-Fe_2O_3 Nanoparticles

The whole process of iron nanoparticle synthesis was used according to Pant et al. (2009). The whole procedure of α-Fe_2O_3 synthesis is represented in the form of a flow diagram in Fig. 1. The chemicals used for the synthesis of α-Fe_2O_3 were ferric nitrate anhydrous and oxalic acid dehydrates of analytical grade without any further purification. Nano powder synthesis process was carried out by mixing ferric nitrate and oxalic acid aqueous solutions in a molar ratio of 3:1 and stimulated at room temperature for one hour with the help of a magnetic stirrer (Fig. 2). Evaporation of this mixture was done by heating on a hot plate at temperature ~ 125°C and a greenish yellow colored precursor was formed. Further drying of the precursor formed was performed for about 1 h until the color changed from greenish yellow to dark brown. The dark brown precursor was ground to make iron oxide powder, followed by calcination for 2 and a half hours at temperatures ranging from 250-450°C.

Characterization of Synthesized α-Fe_2O_3 Nanoparticles

The prepared α-Fe_2O_3 nanoparticles were characterized with the help of instruments like XRD, SEM-EDS, FTIR, Raman spectrometer, and BET for structure and surface morphological properties and size specification of the synthesized α-Fe_2O_3 nanoparticles. An X-ray diffractometer was used to record spectra of the synthesized α-Fe_2O_3 nanoparticles for identifying the structural phase and to estimate particle size. The model used for the analysis was the Rigaku Miniflex-II diffractometer, Japan. Scanning electron microscopy (SEM) was used for morphological structure analysis of synthesized α-Fe_2O_3 nanoparticles by using an instrument with model number JSM 7610 F+, JEOL, Japan, operated at an accelerating voltage of 15kV. EDS measurement was done for the estimation of the chemical composition of the prepared sample's weight and atomic percentage. The BET analysis was performed by using Micromeritics Gemini V2.00.

The Raman spectra were recorded by a Raman spectrometer (Alpha 300, WITec Focus Innovations with an Excitation laser line of 632 nm from a He-Ne laser) at room temperature. Fourier transform infrared (FT-IR) spectra were recorded by using Spectrum Two, PerkinElmer in a range of 400 cm^{-1} to 4000 cm^{-1} wavenumbers for identifying the chemical bonds along with the functional group of the

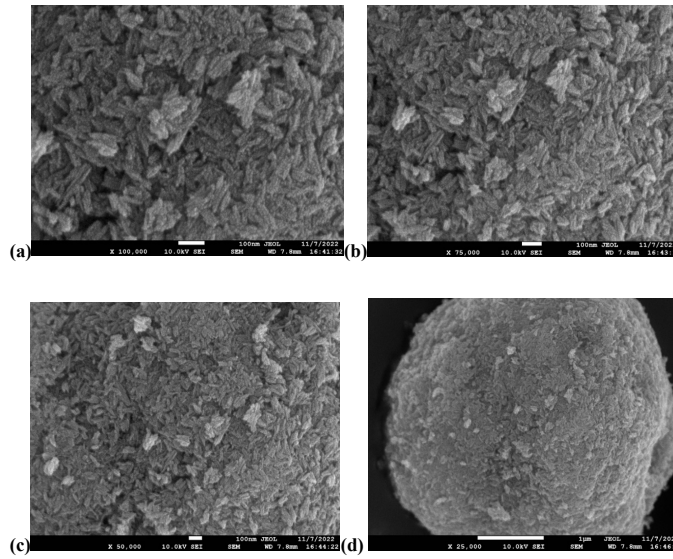

(e)

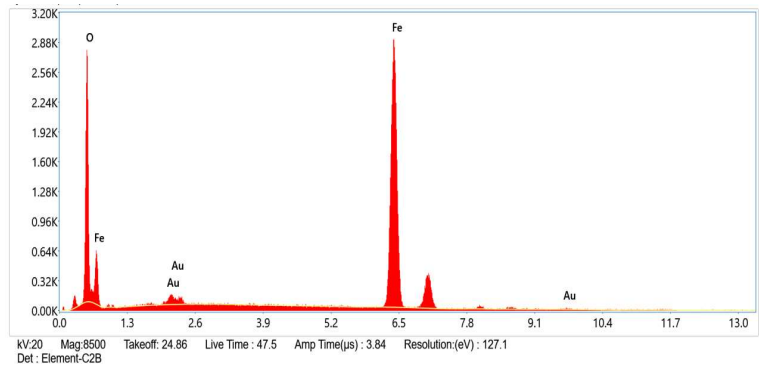

(f)

Element	Weight (%)	Atomic (%)	Error (%)	R	A	F
O K	30.9	62.0	9.9	0.8401	0.1836	1.0000
Fe K	64.8	37.3	2.5	0.9256	0.9593	1.0322
Au L	4.3	0.7	34.4	0.9660	0.9541	1.0231

Fig. 3: SEM-EDS analysis of α-Fe_2O_3 nanoparticles. (a) SEM image of α-Fe_2O_3 nanoparticles at 100000 X magnification; (b) SEM image of α-Fe_2O_3 nanoparticles at 75000 X magnification; (c) SEM image of α-Fe_2O_3 nanoparticles at 50000 X magnification; (d) SEM image of α-Fe_2O_3 nanoparticles at 25000 X magniIation; (e) depiction of EDS peaks of the elements in α-Fe_2O_3 nanoparticles; (f) Weight percentage of the elements in α-Fe_2O_3 nanoparticles.

synthesized α-Fe_2O_3 nanoparticles. Differential Scanning Calorimetry (DSC) was used for differential scanning calorimetry examination and the thermal stability of α-Fe_2O_3 nanoparticles between 0-500°C under a nitrogen atmosphere with an increase in temperature of 10°C.min^{-1}. The model used was Discovery 25/TA Instruments Waters. Zeta potential was measured with a Malvern Zeta analyzer.

RESULTS AND DISCUSSION

SEM-EDX Analysis

A scanning electron microscope (SEM) is a type of microscope that provides high-resolution images of any sample or object by scanning it with a focused beam of electrons across the surface and detecting backscattered electron signal with up to ~50000 X magnifications (Nahari et al. 2022). Energy-dispersive X-ray spectroscopy (EDX or EDXS), also known as Energy dispersive X-ray analyzer (EDA) or energy dispersive X-ray microanalysis (EDXM), is an analytical technique used to provide the elemental analysis, quantitative composition, and chemical composition of a sample (Sayed & Polshettiwar 2015). Scanning Electron Microscopy was used for the qualitative analysis of surface morphology and structure of calcined α-Fe_2O_3 nanoparticles (Fig. 3). In Fig. 3(a-d), α-Fe_2O_3 nanoparticles images at different magnifications at the nanoscale are shown. The assembly of α-Fe_2O_3 nanoparticles was compact, having a spherical or rhombohedral (hexagonal) structure. The synthesis of α-Fe_2O_3 nanoparticles had a diameter in the range of 9 nm-12.5 nm.

Energy dispersive spectroscopy (EDS) of α-Fe_2O_3 prepared by the simple chemical method is depicted in Fig. 1, which confirms the presence of iron and oxygen elements with their weight percentage in the synthesized sample. The presence of gold (Au) is because of the gold coating on the sample during the SEM analysis. The peaks of iron and oxygen are shown in the EDS graph with fewer other elements as impurities. The atomic percentage of iron and oxygen in the sample was 37.3% and 62%, respectively. The weight percentage of iron and oxygen was 64.8% and 30.9%, respectively, as shown in Fig. 3(f).

FTIR Analysis

Fourier Transformed Infrared Spectroscopy (FTIR) was used to investigate the functional groups of the synthesized α-Fe_2O_3 nanoparticles. Fig. 4 depicts the infrared spectrum of the synthesized α-Fe_2O_3 nanoparticles. The spectrum represents various kinds of chemical bonds and their functional groups present in the synthesized α-Fe_2O_3 sample. The broader band located at 3409.78 cm^{-1} wavenumbers is assigned to the O–H stretching vibration, which indicates a hydrogen bond and confirms the presence of the hydroxyl (-OH) group (Weldegebrieal & Sibhatu 2021). The stretching and bending vibration peak located at 1631.12 cm^{-1} wavenumbers represents the H-O-H bond of adsorbed water (Subaihi & Naglah 2022).

The spectrum of α-Fe_2O_3 confirmed the presence of the aromatic C-H in-plane bend stretching vibrations observed at peaks 1023.80 cm^{-1} and 1093.22 cm^{-1} (Khoshnam et al. 2021). The absorption bands at 446.42 cm^{-1} and 531.26 cm^{-1}

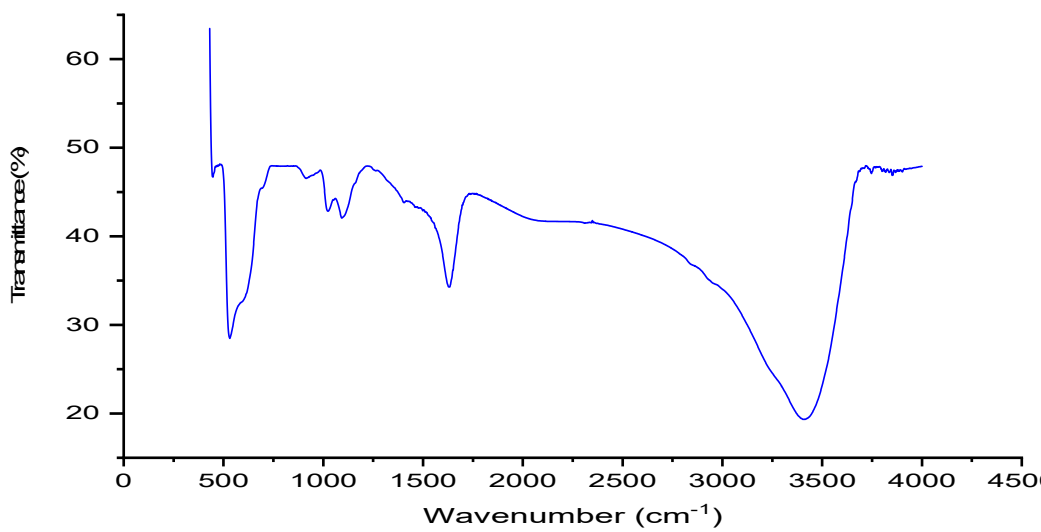

Fig. 4: Fourier Transformed Infrared Spectroscopy (FTIR) analysis of α-Fe_2O_3 nanoparticles.

signify the vibrations of the Fe-O stretching bond, which confirms the presence of α-Fe_2O_3 (Khoshnam et al. 2021).

XRD Analysis

X-ray diffraction (XRD) examination of peaks of the synthesized α-Fe_2O_3 nanoparticles was studied and shown in Fig 5. The synthesized iron oxide nanoparticles were identified as α-Fe_2O_3 (Hematite) on evaluation of the obtained spectra against the Joint Committee on Powder Diffraction Standards Database (JCPDS) manual. With the increase in temperature, the diffraction peak intensity of the samples also increases and decreases in the peak width at half maximum, indicating an improvement in crystallinity (Gurlhosur & Sreekanth 2018). The XRD pattern of the sample shows the high crystallinity of the α-Fe_2O_3 sample.

The peaks at 2θ were obtained at 30.46°, 35.86°, 43.46°, 57.46° and 63.14° as per ASTM standard for α-Fe_2O_3 nanoparticles. The peaks obtained are typical of hematite and are in relevance with (Shah 2023.), which obtained α-Fe_2O_3 nanoparticles using glucose and sucrose fuels. The XRD peaks are good indicators of the rhombohedral hematite, related to the R3c space group with unit cell parameters of a = 5.038 Å and c = 13.772 Å. Moreover, the XRD results also showed more intense and sharper peaks, which indicates the high crystalline nature of the α-Fe_2O_3 (Benhammada et al. 2020, Khoshnam et al. 2021).

Raman Analysis

Raman spectroscopy is a significant non-destructive tool to investigate the chemical and structural composition of a wide range of materials. It has been regarded as the appropriate technique for the characterization of nano-sized substances since it allows the identification of slight vibrations of nonmaterial (Benhammada et al. 2020). To further clarify the phase of the rhombohedral particles, Fig. 6 shows the Raman spectrum of the synthesized α-Fe_2O_3 nanoparticles. The spectrum of synthesized α-Fe_2O_3 nanoparticles shows three strong peaks around 227, 289, and 401 cm^{-1} and two weak bands at 494 and 601 cm^{-1}. The results are in accordance with Kumar et al. (2023). Also, the two strong peaks at 227 and 289 cm^{-1} can be attributed to the A_1g and E_g Raman modes of α-Fe_2O_3 nanoparticles, which are very near to 224 and 287 cm^{-1} peaks obtained by (Rohilla et al. 2023, Abad et al. 2020). The different vibrational modes of the material are presented.

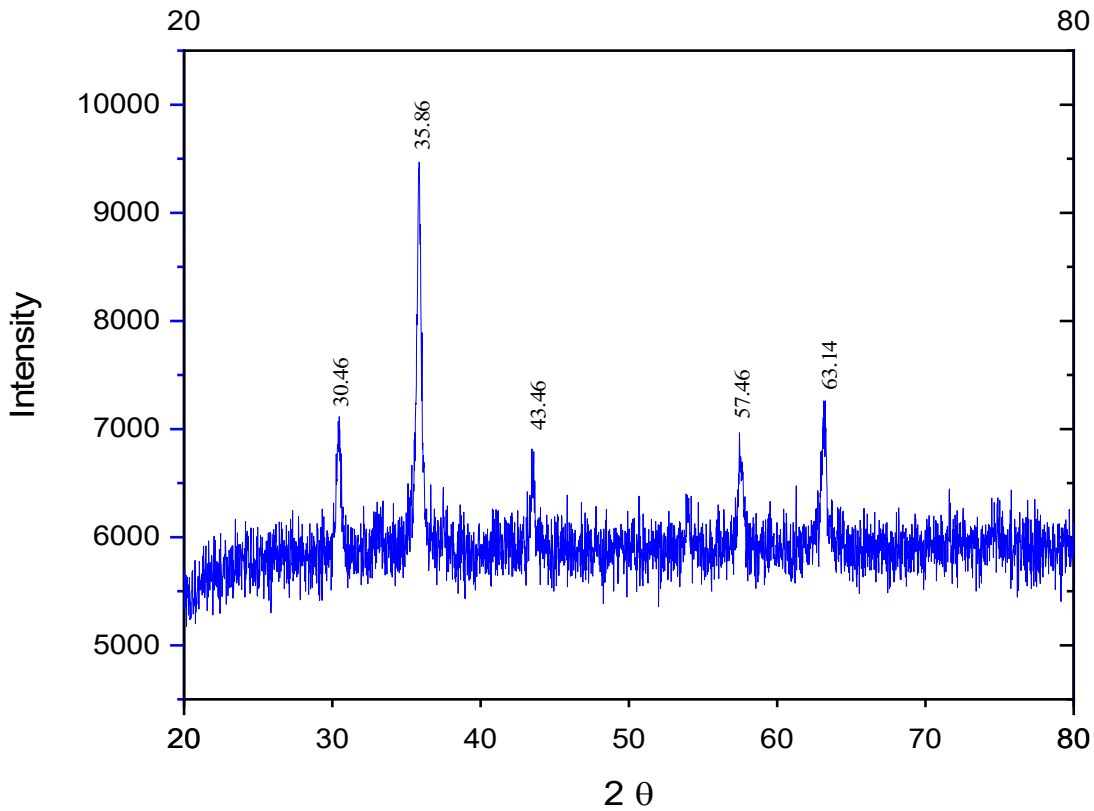

Fig. 5: X-ray Diffraction (XRD) pattern of synthesized α-Fe_2O_3 nanoparticles.

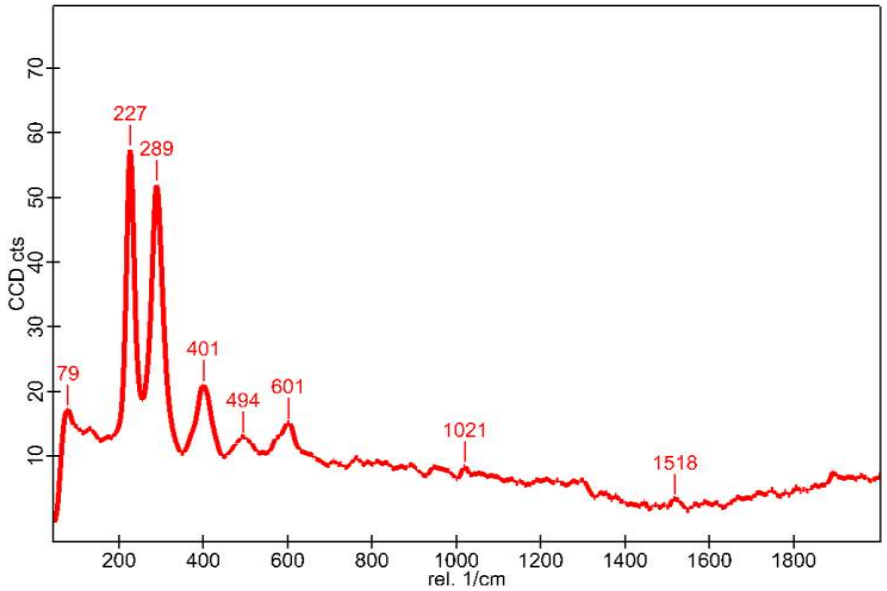

Fig. 6: Raman spectroscopy of synthesized α-Fe_2O_3 nanoparticles.

DSC Analysis

In Differential Scanning Calorimetry (DSC) analysis, the relationship between heat flow (W/g) and temperature (°C) is analyzed for the synthesized α-Fe_2O_3 nanoparticles. The DSC results are depicted in Fig. 7. The two main peaks observed were an endothermic peak at a temperature of 156.62°C with normalized enthalpy of 121.10 $J.g^{-1}$ and an exothermic peak at a temperature of 332.37°C with normalized enthalpy of 35.105 $J.g^{-1}$. The endothermic peak is associated with a phase change in the sample, which indicates that the degradation of the sample can occur at a small range of temperatures. An exothermic peak at 332.37°C showed a big step change, which indicates the stability of the sample and phase transition started. These peaks are related to the transformation of the amorphous phase to crystalline Fe_2O_3 and its transformation to α-Fe_2O_3 nanoparticles (Bozkurt 2020). The DSC profile confirms the purity of the α-Fe_2O_3 nanoparticle synthesized.

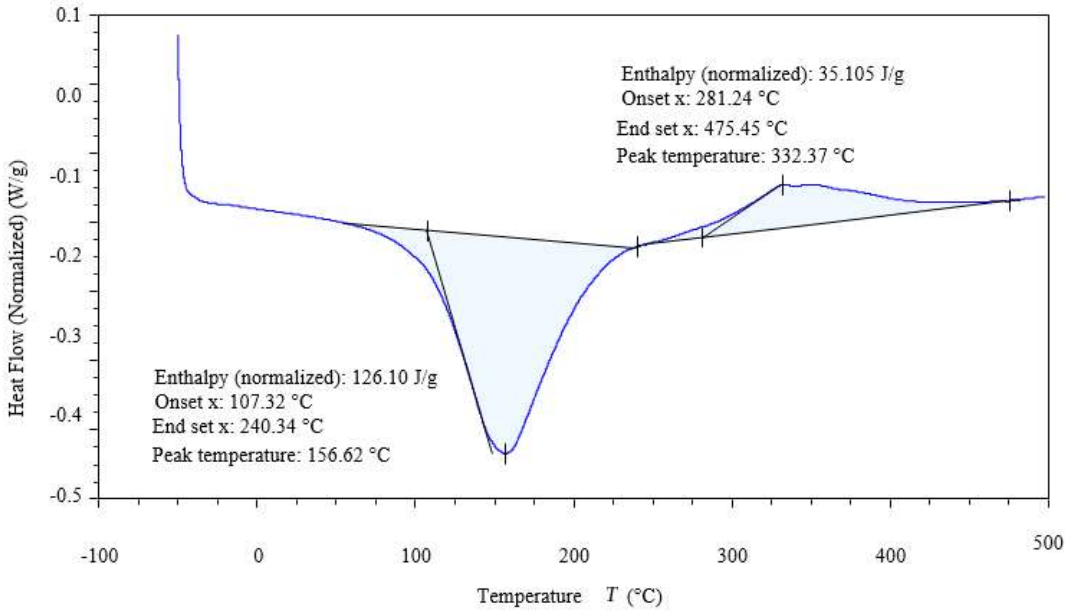

Fig. 7: Differential Scanning Calorimetry (DSC) graph of α-Fe_2O_3 nanoparticles.

Table 1: Zeta potential deviation and parameters.

		Mean [mV]	Area [%]	Standard deviation
Zeta potential [mV]	-15.0	Peak 1: −15.0	100.0	3.29
Zeta deviation [mV]	3.15	Peak 2: zero	zero	Zero
Conductivity [mS.cm^{-1}]	0.320	Peak 3: zero	zero	Zero
Quality of the result	Good			

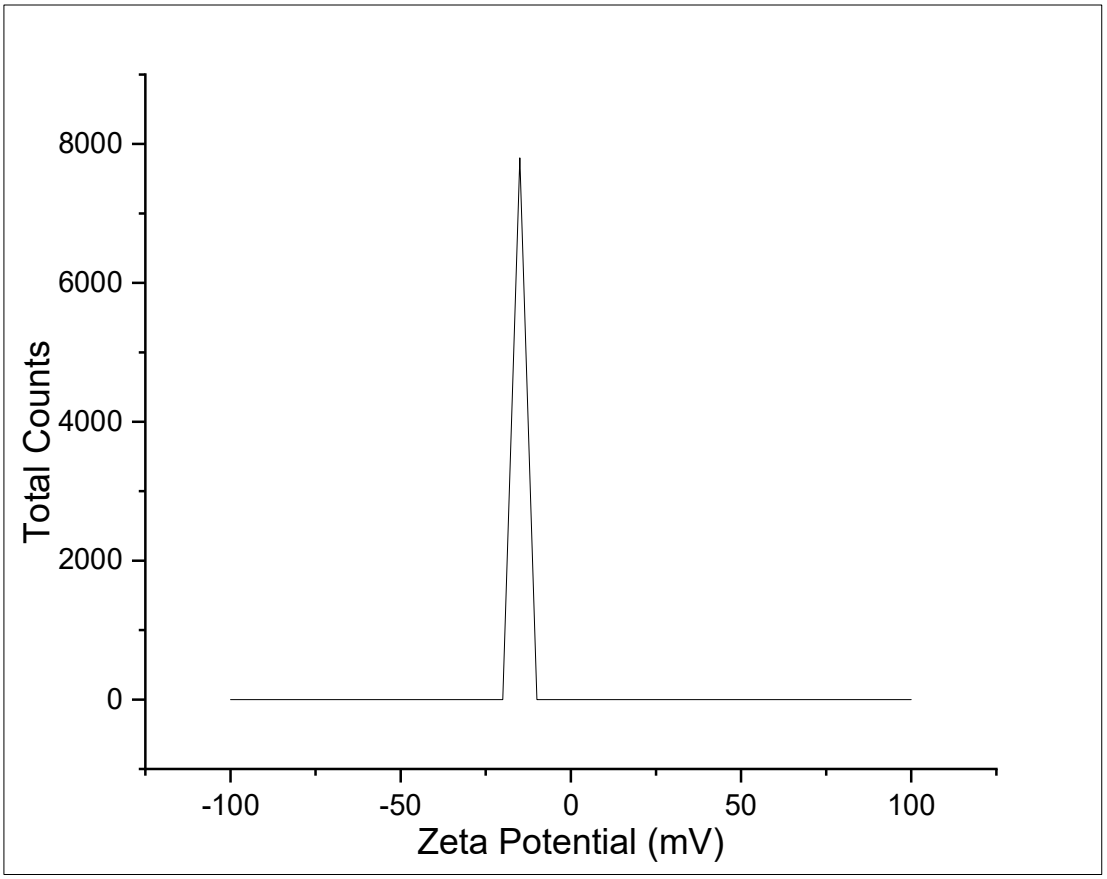

Fig. 8: Zeta potential of synthesized α-Fe_2O_3 nanoparticles.

Zeta Potential

Size is one of the most important factors in describing nanoparticle (NP) properties, although to distinguish NPs from bulk materials, substantial discussion exists on the size threshold (Lakshminarayanan et al. 2021). ζ-potential is the electrokinetic potential difference between the diffusing medium and compact layer of fluid in which nanoparticles are immersed (Kongsat et al. 2021). ζ-potential measurements were performed for the assessment of colloidal and dispersion stability. At a low ζ-potential value, dispersions in due course are cumulative because of the van der Waals force. Thus, NPs with a high absolute value of ζ-potentials are supposed to have stable dispersions, whereas those with lower values lean toward accumulation (Colla et al. 2012, Nourafkan et al. 2017). ζ-potential is used to measure the stability (ζ-potential values with greater than +30 mV and less than −30 mV) of nanoparticles in an aqueous solution. ζ-potential was measured using water as a dispersant, with a refractive index of 1.330, a dispersant dielectric constant of 78.5, and a viscosity (cP) of 0.8872. A ζ-potential of −15 mV was measured for the synthesized α-Fe_2O_3 nanoparticles, as shown in Fig. 8 and ζ-potential deviation and parameters are given in Table 1. Thus, the synthesized α-Fe_2O_3 nanoparticles are supposed to have stable dispersal potential. These negative potential charge values suggest that α-Fe_2O_3 nanoparticles can be good adsorbents for various applications.

Table 2: BET surface area of α-Fe_2O_3 nanoparticles as reported by various studies.

Method of NP synthesis	BET surface area [$m^2.g^{-1}$]	References
Chemical synthesis	79.2	(Maji et al. 2012)
Chemical synthesis	90.71	(Waseem et al. 2014)
Chemical synthesis	105.1	(Zhang et al. 2012)

BET Analysis

The N_2 adsorption-desorption isotherm characteristics were used to estimate the porous structure of the α-Fe_2O_3 nanoparticles. The BET surface area of the α-Fe_2O_3 nanoparticles was calculated as 132.9304 $m^2.g^{-1}$, which is significantly higher than the values previously reported by various chemical methods (Table 2). The pore volume of α-Fe_2O_3 nanoparticles was measured as 0.379642 $cm^3.g^{-1}$. The greater specific surface area and microporous characteristics of α-Fe_2O_3 nanoparticles would be advantageous for prospective catalytic/adsorptive usage of this substance in a variety of environmental applications.

CONCLUSION

The iron oxide nanoparticles were synthesized by a simple co-precipitation method at 450°C. The experimental design uses the simplest approach for the preparation of the α-Fe_2O_3 nanoparticles. The characterizations observed showed confirmation of the preparation of good quality α-Fe_2O_3 nanoparticles. The BET surface area of the α-Fe_2O_3 nanoparticles was 132.9304 $m^2.g^{-1}$, which is significantly higher than the other studies reported so far. The XRD spectrum confirms the rhombohedral (hexagonal) structure of α-Fe_2O_3 with highlighted peaks at 30.46°, 35.86°, 43.46°, 57.46° and 63.14°. Further, SEM also confirms the sphere-like or rhombohedral (hexagonal) shape of the characteristic nanoparticles. Moreover, the presence of iron and oxygen is confirmed by SEM-EDS. FTIR provided good quality peaks between the range of 400 cm^{-1} to 4000 cm^{-1} wavenumbers, which represented various kinds of chemical bonds and their functional groups. This also confirmed the presence of the α-Fe-O stretching mode of α-Fe_2O_3 nanoparticles. The Raman spectroscopy showed the phase change in synthesized α-Fe_2O_3 nanoparticles. The DSC analysis showed two peaks, i.e., endothermic and exothermic, confirming the phase transition and stability of the synthesized α-Fe_2O_3 nanoparticles. This further suggests that these nanoparticles can be useful in the absorption process used for wastewater treatment and enhancement of microbial diversity during anaerobic digestion, which ultimately helps in the increment of biogas production and many more applications.

REFERENCES

Abad, Z.A.K., Nemati, A., Khachatourian, A.M. and Golmohammad, M. 2020. Synthesis and characterization of rGO/Fe_2O_3 nanocomposite as an efficient supercapacitor electrode material. J. Mater. Sci. Mater. Electron., 31: 14998-15005. https://doi.org/10.1007/s10854-020-04062-7.

Ansari, M.J., Kadhim, M.M., Hussein, B.A., Lafta, H.A. and Kianfar, E. 2022. Synthesis and stability of magnetic nanoparticles. BioNanoSci., 12(2): 627-638. https://doi.org/10.1007/S12668-022-00947-5.

Aragaw, T.A., Bogale, F.M. and Aragaw, B.A. 2021. Iron-based nanoparticles in wastewater treatment: A review on synthesis methods, applications, and removal mechanisms. J. Saudi Chem. Soc., 25(8): 101280. https://doi.org/10.1016/j.jscs.2021.101280.

Basavegowda, N., Mishra, K. and Lee, Y.R. 2017. Synthesis, characterization, and catalytic applications of hematite (α- Fe_2O_3) nanoparticles as reusable nanocatalyst. Adv. Nat. Sci. Nanosci. Nanotechnol., 8(2): 025017. https://doi.org/10.1088/2043-6254/aa6885.

Benhammada, A., Trache, D., Kesraoui, M., Tarchoun, A.F., Chelouche, S. and Mezroua, A. 2020. Synthesis and characterization of α- Fe_2O_3 nanoparticles from different precursors and their catalytic effect on the thermal decomposition of nitrocellulose. Thermochim. Acta., 686: 178570. https://doi.org/10.1016/j.tca.2020.178570.

Bozkurt, G. 2020. Synthesis and characterization of α- Fe_2O_3 nanoparticles by microemulsion method. Erzincan Univ. J> Sci. Technol., 13: 890-897. https://doi.org/10.18185/erzifbed.742160.

Cao, D., He, P. and Hu, N. 2003. Electrochemical biosensors utilizing electron transfer in heme proteins immobilized on Fe_3O_4 nanoparticles. Analyst, 128(10): 1268-1274. https://doi.org/10.1039/B308242C.

Chircov, C. and Vasile, B.S. 2022. New Approaches in Synthesis and Characterization Methods of Iron Oxide Nanoparticles. In Huang, X.L.E. (eds), Iron Oxide Nanoparticles. Intechopen, NY, pp. 78-104. DOI: 10.5772/intechopen.101784.

Colla, L., Fedele, L., Scattolini, M. and Bobbo, S. 2012. Water-based Fe_2O_3 nanofluid characterization: thermal conductivity and viscosity measurements and correlation. Adv. Mech. Eng., 4: 674947. https://doi.org/10.1155/2012/674947.

Ebrahiminezhad, A., Bagheri, M., Taghizadeh, S.M., Berenjian, A. and Ghasemi, Y. 2016. Biomimetic synthesis of silver nanoparticles using microalgal secretory carbohydrates as a novel anticancer and antimicrobial. Adv. Nat. Sci.: Nanosci. Nanotechnol., 7: 015018. https://doi.org/10.1088/2043-6262/7/1/015018.

Farahmandjou, M. and Soflaee, F. 2015. Synthesis and characterization of α- Fe_2O_3 nanoparticles by simple co-precipitation method. Phys. Chem. Res., 3: 191-196. https://doi.org/10.22036/PCR.2015.9193.

Ganguli, A.K. and Tokeer, A. 2007. Nanorods of iron oxalate synthesized using reverse micelles: Facile route for α-Fe_2O_3 and Fe_2O_4 nanoparticles. J. Nanosci. Nanotechnol., 7: 2029-2035. https://doi.org/10.1166/jnn.2007.763.1.

Gurlhosur, S.H. and Sreekanth, B. 2018. Synthesis characterization of iron oxide (α-Fe2O3) nanoparticles and its application in photocatalytic reduction of cadmium (II). Int. J. Eng. Res. Technol., 7: 388-393. https://doi.org/10.14419/ijet.v7i3.34.19234.

Khoshnam, M., Farahbakhsh, J., Zargar, M. and Mohammad, A.W. 2021. α-Fe_2O_3/graphene oxide powder and thin film nanocomposites as peculiar photocatalysts for dye removal from wastewater. Sci. Rep., 11(1): 20378. https://doi.org/10.1038/s41598-021-99849-x.

Kongsat, P., Kudkaew, K., Tangjai, J., O'Rear, E.A. and Pongprayoon, T. 2021. Synthesis of structure-controlled hematite nanoparticles by a surfactant-assisted hydrothermal method and property analysis. J. Phys. Chem. Solids, 148: 109685. https://doi.org/10.1016/j.jpcs.2020.109685.

Kumar, P., Mathpal, M.C, Inwati, G.K., Kumar, S., Duvenhage, M., Roos, W.D. and Swart, H.C. 2023. Study of defect-induced chemical modifications in spinel zinc-ferrites nanostructures by in-depth XPS

investigation. Magnetochemistry, 9(1): 20. https://doi.org/10.3390/magnetochemistry9010020.

Lakshminarayanan, S., Shereen, M.F., Niraimathi, K.L. and Brindha, P. 2021. One-pot green synthesis of iron oxide nanoparticles from Bauhinia tomentosa: Characterization and application towards synthesis of 1, 3 diolein. Sci. Rep., 11(1): 1-13. https://doi.org/10.1038/s41598-021-87960-y.

Liu, M., Huang, W., Wang, Z., Wu, S. and Liu, R. 2019. A novel rapid-combustion process for the preparation of magnetic α-Fe2O3 nanoparticles. AIP Adv., 9: 0-6. https://doi.org/10.1063/1.5126660.

Lo, H.M., Chiu, H.Y., Lo, S.W. and Lo, F.C. 2012. Effects of micro-nano and non-micro-nano MSWI ashes addition on MSW anaerobic digestion. Bioresour. Technol., 114: 90-94. https://doi.org/10.1016/j.biortech.2012.03.002.

Maji, S.K., Mukherjee, N., Mondal, A. and Adhikary, B. 2012. Synthesis, characterization and photocatalytic activity of α- Fe_2O_3 nanoparticles. Polyhedron, 33: 145-149. https://doi.org/10.1016/j.poly.2011.11.017.

Masoomi, M.Y., Mahmoudi, G. and Morsali, A. 2010. Sonochemical syntheses and characterization of new nanorod crystals of mercury (II) metal-organic polymer generated from polyimine ligands. J. Coord. Chem., 63: 1186-1193. https://doi.org/10.1080/00958971003721226.

Morais, V.A., Verstreken, P., Roethig, A., Smet, J., Snellinx, A., Vanbrabant, M., Haddad, D., Frezza, C., Mandemakers, W., Vogt-Weisenhorn, D., Van Coster, R., Wurst, W., Scorrano, L. and De Strooper, B. 2009. Parkinson's disease mutations in PINK1 result in decreased Complex I activity and deficient synaptic function. EMBO Mol. Med., 1: 99-111. https://doi.org/10.1002/emmm.200900006.

Nahari, M.H., al Ali, A., Asiri, A., Mahnashi, M.H., Shaikh, I.A., Shettar, A.K. and Hoskeri, J. 2022. Green synthesis and characterization of Iron nanoparticles synthesized from aqueous leaf extract of Vitex leucoxylon and its biomedical applications. Nanomaterials, 12(14): 2404. https://doi.org/10.3390/nano12142404.

Nourafkan, E., Asachi, M., Gao, H., Raza, G. and Wen, D. 2017. Synthesis of stable iron oxide nanoparticle dispersions in high ionic media. J. Ind. Eng. Chem., 50: 57-71. https://doi.org/10.1016/j.jiec.2017.01.026.

Pant, P., Naik, B.D. and Ghosh, N.N. 2009. Synthesis of α- Fe_2O_3 nanopowder by simple chemical method. Mater. Technol., 24(4): 213-216. https://doi.org/10.1179/175355509X387183.

Qureshi, A.A., Javed, S., Javed, H.M.A., Jamshaid, M., Ali, U. and Akram, M.A. 2022. Systematic investigation of structural, morphological, thermal, optoelectronic, and magnetic properties of high-purity hematite/magnetite nanoparticles for optoelectronics. Nanomaterials, 12: 1635. https://doi.org/10.3390/nano12101635.

Rao, C.N.R., Kulkarni, G.U., Thomas, P.J. and Edwards, P.P. 2000. Metal nanoparticles and their assemblies. Chem. Soc. Rev., 29: 27-35. https://doi.org/10.1039/A904518J.

Rohilla, M., Saxena, A. and Tyagi, Y.K. 2023. Facile synthesis of rGO/Fe_2O_3 nanocomposite and its combination with aerosol forming composite for ultra-fast fire extinguishment. J. Mater. Sci., 1-16. https://doi.org/10.1007/S10853-022-08130-7.

Sayed, F.N. and Polshettiwar, V. 2015. Facile and sustainable synthesis of shaped iron oxide nanoparticles: Effect of iron precursor salts on the shapes of iron oxides. Sci. Rep., 5(1): 9733. https://doi.org/10.1038/srep09733.

Shah, R.K., 2023. Efficient photocatalytic degradation of methyl orange dye using facilely synthesized α- Fe_2O_3 nanoparticles. Arab. J. Chem., 16(2): 104444. https://doi.org/10.1016/j.arabjc.2022.104444.

Subaihi, A. and Naglah, A.M. 2022. Facile synthesis and characterization of Fe_2O_3 nanoparticles using L-lysine and L-serine for efficient photocatalytic degradation of methylene blue dye. Arab. J. Chem., 15: 103613. https://doi.org/10.1016/j.arabjc.2021.103613.

Terayama, K., Yamashita, T., Oguchi, T. and Tsuda, K. 2018. Fine-grained optimization method for crystal structure prediction. NPJ Comput. Mater., 4: 32. https://doi.org/10.1038/s41524-018-0090-y.

Terna, A.D., Elemike, E.E., Mbonu, J.I., Osafile, O.E. and Ezeani, R.O. 2021. The future of semiconductors nanoparticles: Synthesis, properties and applications. MSEB, 272: 115363. https://doi.org/10.1016/j.mseb.2021.115363.

Villanueva, A., Cãete, M., Roca, A.G., Calero, M., Veintemillas-Verdaguer, S., Serna, C.J., Del Puerto Morales, M. and Miranda, R. 2009. The influence of surface functionalization on the enhanced internalization of magnetic nanoparticles in cancer cells. Nanotechnology, 20: 115103. https://doi.org/10.1088/0957-4484/20/11/115103.

Wang, B., Wei, Q. and Qu, S. 2013. Synthesis and characterization of uniform and crystalline magnetite nanoparticles via oxidation-precipitation and modified co-precipitation methods. Int. J. Electrochem. Sci., 8: 3786-3793.

Waseem, M., Munsif, S. and Rashid, U. 2014. Physical properties of α-Fe_2O_3 nanoparticles fabricated by modified hydrolysis technique. Appl. Nanosci., 4: 643-648. https://doi.org/10.1007/s13204-013-0240-y.

Weldegebrieal, G.K. and Sibhatu, A.K. 2021. Photocatalytic activity of biosynthesized α- Fe_2O_3 nanoparticles for the degradation of methylene blue and methyl orange dyes. Optik, 241: 167226. https://doi.org/10.1016/j.ijleo.2021.167226.

Xu, W., Yang, T., Liu, S., Du, L., Chen, Q., Li, X., Dong, J., Zhang, Z., Lu, S., Gong, Y., Zhou, L., Liu, Y. and Tan, X. 2022. Insights into the synthesis, types and application of iron nanoparticles: The overlooked significance of environmental effects. Environ. Int., 158: 106980. https://doi.org/10.1016/j.envint.2021.106980.

Zhang, G.Y., Feng, Y., Xu, Y.Y., Gao, D.Z. and Sun, Y.Q. 2012. Controlled synthesis of mesoporous α- Fe_2O_3 nanorods and visible light photocatalytic property. Mater. Res. Bull., 47: 625-630. https://doi.org/10.1016/j.materresbull.2011.12.032.